IEEE Robotics and Automation Letters (RAL) paper presented at
2024 IEEE/RSJ International Conference on Intelligent Robots and Systems (IROS)
October 14-18, 2024. Abu Dhabi, UAE

Enhancing Elderly Mobility: A Sturdy, Two-Body Robot for Handlebar Placement in Any Location

Roberto Bolli Jr. and H. Harry Asada[1]

***Abstract*— Grab bars are widely used to provide elderly persons with support for daily activities, but their utility is limited by room geometry, cost of installation, and potential obstruction of other movements. We address these challenges through a mobile robot that can place a handlebar at any point in space, to optimally support postural transitions. Informed by a survey of elderly people and care professionals, we propose a novel two-body robot structure, consisting of two small-footprint mobile bases connected by a four bar linkage. Kinematic analysis shows that the structure can bear the entire weight of a human body, and provides secure support without sliding or tipping. The robot has a minimum width of 29.2 cm to be maneuverable within confined spaces, making it likely the slimmest robot ever developed for mobile postural assistance. A control plan for geometric path tracking is proposed that is generalizable to all robots with two coupled, nonholonomic, mobile bases. This consists of a leader-follower scheme as well as various enhancements to path tracking and dead reckoning that allow the robot to accurately follow a series of waypoints. On an 0.4 meter long test path, despite significant tread slippage, a 1:4 scale model of the robot achieved a root mean square error of 0.01 m and a deviation of 0.015 m from the path terminus, using only the encoders on the treads and robot frame. Finally, the robot's utility for supporting activities of daily living is demonstrated as a proof of concept.**

***Index Terms*— Physically Assistive Devices, Domestic Robotics, Nonholonomic Mechanisms and Systems.**

I. Introduction

The rapid increase in the elderly population, driven primarily by higher life expectancies and advances in medicine, has ushered in a myriad of challenges [1]. One of the most prominent is the shortage of caregivers capable of delivering high-quality care to the aging population. In the U.S., approximately 800,000 elderly people are on waiting lists for subsidized care due to a lack of available workers [2]. Yet the caregiver shortage is only expected to become worse over the next decade, with a projected need for 25% more caregivers in 2031, translating to 700,000 caregiver openings for each upcoming year [3]. Along with other factors, this has led to persistent sub-quality care for seniors, which prompted the White House to issue an executive order on April 18, 2023 to "improve support for caregivers ... and provide more care options for families [4]."

To address these concerns, many robotic devices have been proposed over the past two decades to augment the work of caregivers [5], [6]. These range in function from social companions to item retrievers [7], health monitors, and mobility assistants. Promising results have been reported in enhancing the well-being of elderly people and decreasing the workload of their caregivers [7]. In particular, assistance with mobility is key to preserving the independence of older adults in daily activities. A few relevant eldercare robots are listed below.

(a) MOVAID (b) Pearl (c) Care-o-bot I (d) Care-o-bot II

(e) Monimad (f) RobuWalker (g) RobuMate (h) MOBISERV

Fig. 1. An overview of eldercare mobility and service robots, adapted from [5]. Note the homogeneity in design: the robots' girth impedes their ability to navigate effectively through cluttered environments, and they cannot extend across obstacles such as the lip of a bathtub.

Kompaï was equipped with a small handle to help the user stand up, as well as handlebars enabling use as a walker [8]. Robots such as MOVAID and Pearl (Fig. 1a and b) were able to navigate a controlled household environment, and in the case of Pearl, to assist the user with ambulation. [5] These three robots were limited in the sense that the handlebar was located well within the robots' base of support, so the user needed to reach over and lean into the robot. RobuWalker (Fig. 1f) addressed this issue by the use of a U-shaped base, and was able to help the user perform a sit-to-stand transition [9]. Most other eldercare robots that assist with mobility have similar designs, consisting of either a pedestal with a handlebar or a mechanized walker (Fig. 1). While these prior works demonstrated efficacy in assisting elderly people, their use was generally limited to very specific scenarios, such as sit-to-stand transitions or ambulation. For robots with a pedestal design, high lateral forces could cause the robot to tip over. Lastly, the wide girth of several of the robots impeded effective navigation around obstacles [5].

To better assist users with multiple activities of daily living, we developed the Handle Anywhere (HA) mobile robot [10], which is to our knowledge the first robot specifically designed to position a grab bar at any location in a room,

[1]Roberto Bolli Jr. and H. Harry Asada are with the Department of Mechanical Engineering at the Massachusetts Institute of Technology, 77 Massachusetts Ave., Cambridge, MA 02139, USA. rbolli@mit.edu, asada@mit.edu

unconstrained by the room layout. Grab bars are commonly used postural support aids for elderly people and have been shown to reduce the incidence of falls [11]. However, grab bar installation is limited by the room geometry, and the optimal location for a bar changes based on the motion of the user (e.g. standing up in a bathtub vs. stepping out of the bathtub). The HA robot had the advantages of:

- Positioning the bar at a biomechanically optimal location for each movement.
- Offering support only when necessary, with the robot moving the handlebar after the motion had been completed to avoid impeding further movements.

While the robot was able to successfully provide teleassistance for postural transitions [10], its girth impeded the navigation of cluttered home environments. In addition, the use of an off-the-shelf robot arm to position the handlebar significantly reduced its load bearing capacity. The U-shaped chassis was excellent for assisting with activities where the user could stand inside of the chassis, but poor at providing support across obstacles such as a bathtub lip or coffee table. The wheels also tended to slip when high lateral force was applied to the handlebar, leading to concerns about stability.

In this paper, we present a novel robot for elderly assistance to overcome these limitations. Our robot, nicknamed the Two Buddy Bot (2BB) due to its two mobile bases, consists of a four-bar linkage spanning between two passively pivoting tread drive chassis. To the best of our knowledge, our kinematic design is unique to eldercare robots and perhaps even in the broader field of mobile robotics. This leads to distinct kinematic properties, including the challenges of path following, which cannot be solved by continuous time-invariant stabilizing feedback [12]. Similar to the HA robot, our target population consists of persons older than 65 who require minimal to intermittent weight-bearing for activities of daily living, which encompasses at least 16.4% of the U.S. elderly population, or more than 5.8 million people [13].

The robot design is discussed in detail in section 2 and modeled mathematically in section 3. Section 4 explores the path following and control scheme as well as localization enhancements unique to this class of nonholonomic robots. We assess the robot's ability to support activities of daily living and follow a trajectory in section 5. Finally, section 6 discusses the potential utility of the robot in augmenting the work of caregivers.

II. Mechanical Design

A. Functional Requirements

We sought to tailor the robot's design to not only address the challenges of navigating a cluttered environment and extending over objects, but also to reflect the needs of elderly people. Accordingly, we initiated a user study with persons over the age of 65 to evaluate the difficulty of everyday tasks and preferred handlebar configurations [14], and consulted previous studies of grab bars in seniors [15] [16]. Our respondents had the most difficulty getting out of a bathtub and reaching for items in drawers and cupboards, compared to other common activities of daily living [14].

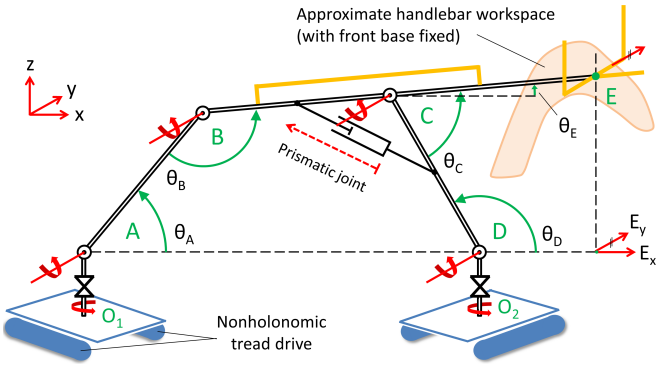

Fig. 2. Kinematic structure of the 2BB in the sagittal (E_x, z) plane.

Our first functional requirement is therefore that the robot must be capable of bearing the entire body weight of an elderly user, since they may offload a significant amount of weight onto the handlebar while standing [15] or leaning down to grab an item. The robot should also be capable of omnidirectional motion to accommodate the small size of many bathrooms and the directional changes that occur when moving from one part of a bathroom to another [16]. The handlebar provided by the robot should be as stable as a grab bar secured to a wall, so the robot drive bases should have a high amount of traction, even on slippery and wet floors.

Furthermore, when asked to perform a sit-to-stand transition with a handlebar in the frontal (coronal) plane, the participants of the user study preferred the bar to be 0.78 $\pm$ 0.05 m off of the floor and 0.61 $\pm$ 0.09 m away from their body (on average, $\pm$ 1 standard deviation) [14]. The workspace of the robot must be able to accommodate these handlebar locations. We also noticed that elderly people commonly placed small tables and other objects in front of chairs. Therefore, the robot frame must be able to span over obstacles to assist in sit-to-stand transfers. The handlebar should be comfortable to grab and sized such that the elderly person can exert a power grip [17]. Finally, for safety, the robot should be able to resist a high lateral force without tipping, as there is no guarantee that the user will only apply downward force on the handlebar.

B. Kinematic Structure

Consider a robot frame comprised of three links connected by revolute joints (Fig. 2). A virtual link between O_1 and O_2 turns the frame into a four-bar linkage. Links BC and CD are attached to a linear actuator which acts as an active prismatic joint. The linear actuator is not backdrivable and, thereby, joint C is rigidly fixed when not powered. This structure allows the handlebar (point E) to extend between 0.71 m and 1.37 m above the ground, meeting the workspace requirement in the previous section. The revolute joint on each end of the linkage (points A and D) is attached to a passive turntable. Each turntable connects via a zero-length link (e.g. $\overline{AO_1} = 0$) to a nonholonomic drive base consisting of two parallel rubber treads. θ_B and θ_C are confined to remain below 180°, preventing the robot frame from entering

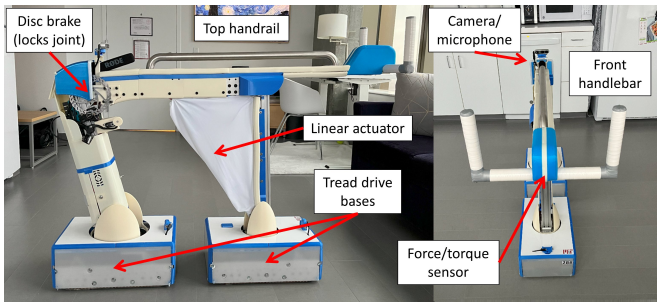

Fig. 3. Side view (left) and front view (right) of the 2BB with protective covers installed, shown in an apartment setting.

any singularities. A long handrail is fixed to the top of the frame, and a triaxial handlebar (Fig. 2, point E) 3.2 cm in diameter is placed at the robot's endpoint. This allows the front handlebar to provide a comfortable power grip for the user from any orientation. Furthermore, the component of the handlebar coaxial with link BC is made to be magnetically retractable, so that when the user is facing the robot, he/she can grab the handlebar without being impeded.

This kinematic structure allows the front handlebar to move omnidirectionally in 3D space using only five actuators: one for each tread and one for the prismatic joint. While the robot system itself is nonholonomic, the passive turntables allow each drive base to rotate in place without displacing the handlebar, which enables the handlebar to be moved in any direction. The two body structure is advantageous for bearing the downward load and load coaxial to link BC (see section 3A), which are the dominant forces exerted during sagittal plane postural transitions such as sit-to-stand [18]. Additionally, the robot forms a virtual closed-loop chain with the ground, which aids in stability.

C. Performance Metrics

Table 1 lists the relevant performance metrics of the prototype robot system shown in Fig. 3. The robot weight and frame dimensions were informed by static analysis of the maximum expected handlebar load (section 3A). Unique to this robot is its ability to support the full weight of a human located outside the base of support of the robot. To our knowledge, this is the only eldercare robot that can achieve such a task at large distances (up to 61 cm from the front base). Additionally, it is the narrowest eldercare robot designed for postural support in the literature, with a minimum width of 29.2 cm when the bases are parallel to the robot frame. This enables a person to walk alongside the robot in a narrow corridor while holding on to the top handlebar for assistance, and aids the robot in navigating between chairs, tables, and other objects. The frame span of 66 cm is wide enough to arch over a coffee table and help a user stand up from a couch or chair.

TABLE I
KEY DIMENSIONS AND PERFORMANCE METRICS

Dimension	Value	Notes
Base width	29.2 cm	Smaller values lead to high shear forces and tread slip during base rotation
Base length	47 cm	Constrained by length of tread
Link AB, BC, and CD	61 cm	
Top of frame length	1.2 m	Distance from B to E
Max / min handlebar height from ground	1.37 / 0.71 m	Encompasses full range of preferred handlebar locations in [14]
Max / min robot length (measured at ground level)	2.67 / 0.94 m	The back of the frame can protrude slightly behind the rear base
Max handlebar span	61 cm	Ground distance from front base to point E; sufficient to extend into a tub or bed
Max frame span	66 cm	Distance from A to D
Robot weight	77 kg	More weight improves traction and increases resistance to tipping over
Max supported weight at front handlebar	100 kg	Dependent on robot configuration; more weight can be supported the farther apart the bases are located
Max axial force before slippage	450 N	Dependent on ground surface; estimated on vinyl tile floor ($\mu = 0.6$)
Max lateral force before tipping	120 N	Average max pull strength of an adult male is 147.6 N [19], and is much lower in elderly persons

III. MODELING

A. Statics

The necessary mass of the robot m_{robot} was determined by a torque balance based on a lateral pull strength of 120 N. The average pull strength of an adult male is 147.6 N [19], and is much lower in elderly persons due to muscle degeneration. Assuming the robot is in the configuration in Fig. 2, when $F_{E_y} = 120N$ is applied at the handlebar E along the $\hat{E}_y$ direction, the ground reaction torque provided by the drive bases is dependent on the distance from the CoM of the robot to the side of each base, $d_{\text{CoM to side}}$. The robot is narrowest when both drive bases are parallel to the frame, as they are in Fig. 3, which means the minimum value of $d_{\text{CoM to side}}$ = base width divided by 2 = 14.6 cm. Balancing the moments in the (E_y, z) plane, where g represents the acceleration due to gravity and $\hat{z}$ is the z-axis unit vector,

$$m_{robot}\, g\, d_{\text{CoM to side}} - F_{E_y}\,(\overrightarrow{O_2E} \cdot \hat{z}) = 0 \tag{1}$$

$$m_{robot} = \frac{F_{E_y}\,(\overrightarrow{O_2E} \cdot \hat{z})}{g\, d_{\text{CoM to side}}} = 75kg$$

It was discovered that placing a large downward force F_z and/or horizontal force F_{E_x} on the handlebar would cause the rear base to slide to its neutral position, where link AB is vertical. This is because any handlebar load in the (E_x, z) plane results in a force F_{AB} axial with link AB, due to the moment about the front base O_2. F_{AB} leads to a force $F_{lateral}$ pulling the rear drive base on the ground along $\overrightarrow{AD}$, dependent on θ_A.

$$F_{AB} = \frac{F_{E_x}(\overrightarrow{O_2E} \cdot \hat{z}) - F_z(\overrightarrow{O_2E} \cdot \hat{E}_x)}{\overline{O_2B}} \cdot \hat{\overrightarrow{AB}} \tag{2}$$

$$|F_{lateral}| = F_{AB}\, cos(\theta_A) \tag{3}$$

When $|F_{lateral}|$ is small, friction with the ground prevents the rear base from slipping. Denoting the coefficient of

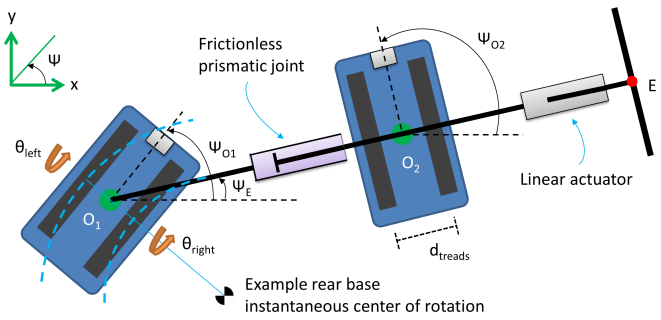

Fig. 4. Kinematic representation of the 2BB in the overhead plane. The four-bar frame linkage is modeled as a frictionless prismatic joint with a linear actuator between the handlebar and front base. The instantaneous center of rotation of each base is dependent on the velocity of each tread.

friction between the treads and the ground as μ, the drive base will not slip as long as

$$|F_{lateral}| \leq \mu \left(m_{base}\, g - F_{AB}\, sin(\theta_A) \right) \tag{4}$$

The mass of each base m_{base} is approximately 32 kg, and the coefficient of friction μ is ≥ 0.5 on most floors (see section 5 for experimental measurements). When $\theta_A = 45°$ as in Fig. 2, the rear base will slide such that link AB becomes vertical if the total downward and horizontal force on the handlebar $(F_z + F_{E_x})$ exceeds around 200 N. To prevent this from occurring, a bicycle disc brake is used to selectively lock joint B (Fig. 3, left) when the front handlebar is grabbed. This effectively turns the three-bar frame into a single rigid body when the brake is active, ensuring that the distance between the bases $\overline{O_1O_2}$ stays constant and the frame does not change configuration under an applied load.

The maximum vertical force F_z the handlebar can bear is dependent on the frame pose and if the brake on joint B is locked. The contribution of the weight of the frame to the moment is negligible and can be ignored. Assuming joint B is locked, a moment balance about O_2 (eq. 5) shows that F_z reaches high values as the ground distance between the handlebar and the front base approaches zero, that is, $(\overrightarrow{O_2E} \cdot \hat{E}_x) \rightarrow 0$. Here, $\hat{E}_x$ represents the direction of link BE along the ground plane xy. $(\overrightarrow{O_2E} \cdot \hat{E}_x)$ is shown in Fig. 2 as the dashed horizontal line between D and the projection of E onto the xy plane. If the materials used to construct the frame are sufficiently strong, the theoretical maximum load bearing capacity approaches infinity as the handlebar moves over the front base, since $\overline{O_2E}$ becomes zero. In the pose shown in Fig. 3, the robot can support around 75 kg.

$$|F_z| \leq \frac{m_{base}\, \overline{O_1O_2}\, g}{(\overrightarrow{O_2E} \cdot \hat{E}_x)} \tag{5}$$

B. Kinematics

Under the assumption that both bases stay in contact with the ground at all times, a virtual link connects joints A and D (dashed line in Fig. 2). This creates the following constraint equations for the robot frame, which can be solved to determine the pose of the frame using only one joint angle.

$$\theta_A + \theta_B - \theta_C - \theta_D = 0 \tag{6}$$

$$\begin{aligned} \overline{AB}\, cos(\theta_A) + \overline{BE}\, cos(\theta_A + \theta_B + \pi) = \\ \overline{AD} + \overline{CD}\, cos(\theta_D) + \overline{CE}\, cos(\theta_D + \theta_C + \pi) \end{aligned} \tag{7}$$

$$\begin{aligned} \overline{AB}\, sin(\theta_A) + \overline{BC}\, sin(\theta_A + \theta_B + \pi) + \\ \overline{CD}\, sin(\theta_A + \theta_B - \theta_C + \pi) = 0 \end{aligned} \tag{8}$$

Because each drive base is nonholonomic, the current pose of one base can only be obtained by integrating the time history of the tread angles, or using forward kinematics if both the location of the other base and the angle of one of the frame joints (θ_A through θ_D) is known. From here, standard kinematic techniques can be used to determine the location of the front handlebar. The rotation of the handlebar about $\hat{E}_x$ (i.e. the pitch) will always be zero, since the kinematic couplings prevent the frame from tilting laterally. Therefore, the handlebar pose can be defined along 5 axes in 3D space.

$$p = [x_E, y_E, z_E, \theta_E, \Psi_E] \tag{9}$$

Despite the system being nonholonomic, there exist one, two, or four unique inverse kinematics solutions for a desired handlebar pose. This is due to the linkage attached to each base (AB and CD) taking one of two possible poses, mirrored about the z axis. If each of the angles θ_B and θ_C are $\geq \pi/2$, the same handlebar pose can be achieved by $\pi - \theta_B$ and $\pi - \theta_C$, respectively. These configurations can be found analytically using the range of motion of each joint (specified in section 2B).

The Jacobian J of the robot system $\dot{p} = J\dot{q}$ can be found by analyzing the robot in the overhead (x, y) and sagittal (E_x, z) planes, as shown in Fig. 2, with

$$\dot{q} = [\dot{\theta}_{O_1,\,left},\, \dot{\theta}_{O_1,\,right},\, \dot{\theta}_{O_2,\,left},\, \dot{\theta}_{O_2,\,right},\, \dot{\theta}_C]$$

where $\dot{\theta}_{O_1,\,left}$ is the angular velocity of the left tread on the rear base. For each drive base b, the Jacobian relative to the global coordinate system is

$$\begin{pmatrix} \dot{x}_b \\ \dot{y}_b \\ \dot{\Psi}_b \end{pmatrix} = \begin{pmatrix} \frac{r_{\text{tread}}\, \cos(\Psi_b)}{2} & \frac{r_{\text{tread}}\, \cos(\Psi_b)}{2} \\ \frac{r_{\text{tread}}\, \sin(\Psi_b)}{2} & \frac{r_{\text{tread}}\, \sin(\Psi_b)}{2} \\ \frac{r_{\text{tread}}}{d_{\text{treads}}} & \frac{r_{\text{tread}}}{d_{\text{treads}}} \end{pmatrix} \begin{pmatrix} \dot{\theta}_{\text{right}} \\ \dot{\theta}_{\text{left}} \end{pmatrix} \tag{10}$$

where r_{treads} is the radius of each tread and d_{treads} is the distance between treads, as shown in Fig. 4. The back base, O_1, causes the endpoint E to rotate about O_2:

$$\begin{pmatrix} \dot{x}_E \\ \dot{y}_E \end{pmatrix} = \begin{pmatrix} \frac{\overline{O_2E}\, \sin(\Psi_{O_1} - \Psi_E)}{\overline{O_1O_2}} & 0 \\ 0 & \frac{\overline{O_2E}\, \sin(\Psi_{O_1} - \Psi_E)}{\overline{O_1O_2}} \end{pmatrix} \begin{pmatrix} \dot{x}_{O_1} \\ \dot{y}_{O_1} \end{pmatrix} \tag{11}$$

The front base O_2 causes the endpoint E to extend radially and rotate around O_1. As in eq. 11, the transformation matrix between $(\dot{x}_{O_2}, \dot{y}_{O_2})$ and $(\dot{x}_E, \dot{y}_E)$ is diagonal, with both non-zero elements equal to

$$\cos(\Psi_{O_2} - \Psi_E)\, \frac{(\overline{O_1O_2} + \overline{O_2E})\, \sin(\Psi_{O_2} - \Psi_E)}{\overline{O_1O_2}} \tag{12}$$

From eq. 10, 11, and 12, we can obtain a Jacobian for the endpoint xy coordinates. The endpoint angle $\dot{\Psi}_E$ is related

to each tread's velocity $\dot{\theta}_{tread}$ by the following expression, which is multiplied by -1 for the rear base.

$$\dot{\Psi}_E = \frac{r_{\text{tread}} \sin\left(\Psi_E - \Psi_{\text{base}}\right)}{2\,\overline{O_1 O_2}}\,\dot{\theta}_{base,\,tread} \qquad (13)$$

Forward kinematic equations relate points O_1 and O_2 to the endpoint height z_E and angle θ_E. From here, the full robot Jacobian can be assembled. Numerical analysis found that it is rank deficient, with the rank degenerated to 3. Specifically, only two of the three 2D ground planar motion coordinates are independent, as is expected from a nonholonomic system, and the yaw of the handlebar (Ψ_E) is dependent entirely on the location of the bases.

IV. Control Scheme

Previous works [12], [20] have developed strategies for path planning, trajectory generation, and trajectory tracking for an active car/passive trailer system. However, only the lead car was powered, and the trailers were connected by passive revolute joints. Work has also been done on trailers that are actively steered [21] but have free spinning wheels. Our robot differs from these systems as each base is actively powered, the treads introduce significant slip, and the four-bar linkage connecting the bases acts as a passive prismatic joint (Fig. 4). Thus, new control methods are necessary, which are generalizable to all robots with two nonholonomic tread drives connected by a variable-length coupling.

Nonholonomic vehicles are frequently globally controllable when linearized about a nonstationary trajectory [22]. However, linearizing about certain poses can lead to a system that is not controllable, and no continuous time-invariant feedback law can stabilize driftless nonholonomic systems [23]. Due to these difficulties, standard motion planning techniques for holonomic systems cannot be directly applied to nonholonomic motion [12]. We thus introduce a trajectory following scheme for the 2BB and several enhancements to dead reckoning. Additional details about the control scheme can be found in the supplementary materials.

A. Path Generation and Trajectory Following

The robot is commanded to follow a series of waypoints via dead reckoning of the tread angles. For simplicity, the front base path is crafted manually (example path shown in Fig. 5). The final front and rear base poses are calculated kinematically based on a desired terminal handlebar pose.

A basic navigation method we call "point and shoot" involves rotating each base to align with the subsequent waypoint and then driving straight towards it. Although this approach is valid in geometric path tracking, the motion is jerky and disjointed, since the bases have to change between pure translation and pure rotation at each waypoint. Here, the goal is to develop a simple algorithm to minimize jerkiness while maintaining path fidelity. We achieve this by shifting the instantaneous center of rotation [24] (see Fig. 4) of each drive base.

1) Sequential waypoints that are either duplicates or very close to each other are removed.

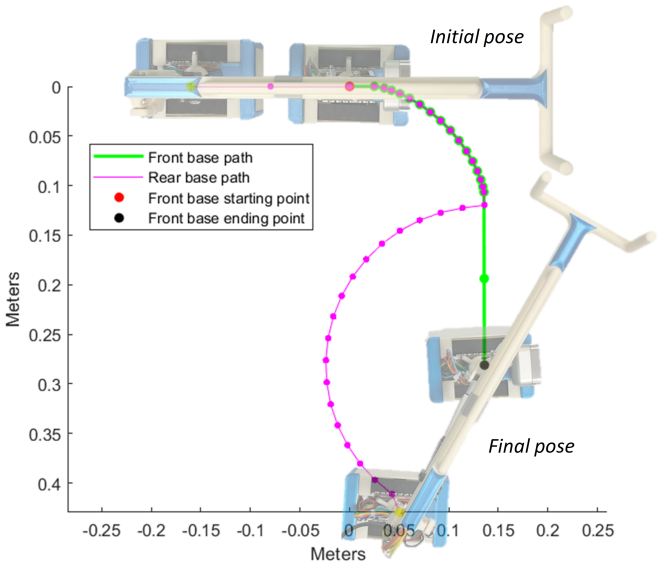

Fig. 5. Example path for the drive bases on a 1:4 scale model of the 2BB. The corresponding initial and final robot pose is overlaid onto the plot.

2) The first three waypoints are loaded into a segment.
3) To find the segment's instantaneous center of rotation, a circle is fit to minimize the squared error. If the points are exactly or nearly linear, a circle of radius r = 1000 meters is used.
4) The base is rotated to be tangent to the circle.
5) The base is driven along the circle from the first to second waypoint.
6) Once the base reaches the second waypoint, steps 3-5 are repeated using a segment comprised of the second waypoint and the two successive waypoints, until the final waypoint is reached.

A dummy waypoint is added to the end of the trajectory since two lookahead points are always required (step 6). While the bases still rotate at each waypoint (step 4), the magnitude of rotation is less than the "point and shoot" method, since part of the rotation is accomplished through following the circular trajectory (step 5). Compared to conventional strategies such as pure pursuit [25], this scheme guarantees that the robot will hit every waypoint. Other reconfigurable robots [26] have found success in modulating the center of rotation to follow a path, under different kinematic and vehicular constraints.

B. Rear Base Coordination

The rear base is commanded to follow the same trajectory as the front base while remaining a nominal distance d_0 behind, causing the robot to slither like a snake. While many alternative coordination strategies exist, this scheme is particularly useful for reducing the width of a path and thereby avoiding collisions with obstacles. Additionally, it is only required to design a single trajectory (the front base) as opposed to two trajectories for both mobile bases.

The minimum and maximum base separation, d_{min} and d_{max}, were calculated from the joints' physical range of

motion, with d_{min} equal to the base length and d_{max} equal to the base length plus the maximum frame span (Table 1). At any point in the trajectory, the frame is being either compressed or elongated by each base, unless the base is stationary or undergoing pure rotation about its centerpoint (O_1 or O_2). This results in a respective decrease or increase in d, the distance between the bases. The magnitude of compression or elongation is dependent on each base's translational velocity $\vec{v}_{trans}$, a column vector that can be obtained from the vehicle Jacobian in eq. 10. We define an indicator variable $\lambda_{base} = sign(\hat{\Psi}_E \cdot \vec{v}_{trans})$, where $\hat{\Psi}_E = [\cos(\Psi_E), \sin(\Psi_E)]$ in the xy plane. λ is multiplied by -1 for the rear base, such that for each base, if $\lambda = 1$, the base's velocity is increasing the distance d between bases, and if $\lambda = -1$, it is decreasing d. We modulate the speed of each base $|v_{base}|$ to be linearly proportional to d minus the nominal base separation d_0, scaled by the base's target speed $|v^0|$.

If $\lambda_{base} > 0$ and $d > d_0, |v_{base}| = |v^0| \frac{d-d_0}{d_{max}-d_0}$

If $\lambda_{base} < 0$ and $d < d_0, |v_{base}| = |v^0| (1 - \frac{d-d_0}{d_{min}-d_0})$

This creates a virtual exponential spring on the distance between the two bases, since the rate of change of the base separation $\dot{d}$ is proportional to d, resulting in a well of stability in the vicinity of d_0. Damping is introduced from friction within the robot system, making it very stable even at high stiffnesses. As d is measured directly using the absolute encoders on the frame joints, the control scheme is fully decoupled from the robot's trajectory unless both bases are commanded to drive towards or away from each other. In such cases, the robot will stop as it approaches d_{max} or d_{min}, since each base's velocity will be decreased to zero.

C. Enhancements to Dead Reckoning

Sensor measurements of the angles of the revolute joints and turntables significantly increase the dead reckoning accuracy of each base. We can exploit kinematic constraints among these sensor readings for improved pose estimates. These strategies are unique to this type of robot. We leverage the fact that the treads only tend to slip if the bases are turning, but provide excellent traction when moving linearly. Precise modelling of the tread slippage, which is difficult due to undulations in the ground surface and the accumulation of debris on the treads, is not required.

- Base angle: When a drive base follows a relatively linear trajectory or remains stationary, implying a nearly constant angle (see Fig. 4), the angle of the other base is updated using the former base's estimated angle and the encoders on the turntables, which measure the base rotation relative to $\overrightarrow{O_1 E}$, i.e., Ψ_{base,O_1E}. For example, $\Psi_{O_1} = \Psi_{O_2} - \Psi_{O_2,O_1E} + \Psi_{O_1,O_1E}$.
- Base position: In the same scenario, the position of one base and the measured frame pose is used to calculate the actual position of the other base. This helps to correct for slippage when the latter base is making a sharp turn. The next few waypoints (corresponding to a path distance of 0.6 m) are shifted by successively smaller intervals to redirect the base to the desired path.

In all other cases, the base position is updated using dead reckoning via tread encoder readings.

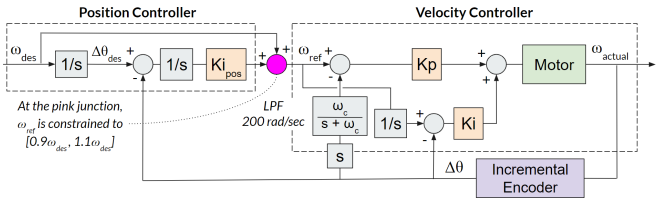

Fig. 6. Tread motor controller. The position controller helped to eliminate steady-state position error by increasing or decreasing the reference velocity by up to 10%. All integrators had anti-windup protection.

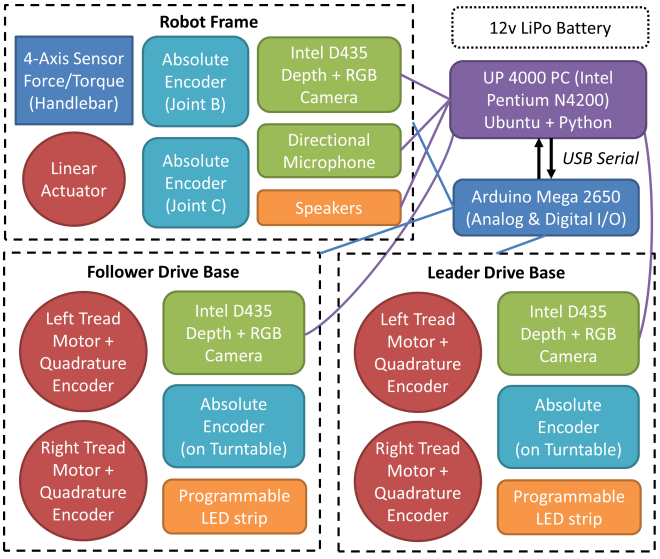

Fig. 7. Block diagram of the 2BB robot system.

D. Low-level Motor Control

Fig. 6 shows the control scheme for each motor, which consists of a proportional-integral velocity controller with a feedforward term and an integral position control outer loop. The position controller is nonlinearly constrained to saturate at ± 10% of the desired tread velocity, which helps to reduce steady-state position error (inherent to PI velocity control) while avoiding large deviations from the intended velocity. To prevent integrator windup, the desired tread angle is reset each time the motor velocity is set to zero.

V. Implementation and Experimental Validation

Each tread drive comprises a urethane rubber timing belt (AndyMark 3963) and three cogs, with the center cog dropped by approximately 0.2 cm to reduce shear forces during base rotations. The tread was driven by two DC motors (AndyMark 3103) and equipped with a quadrature encoder for closed-loop control up to ≈ 0.45 m/s. The robot's coefficient of friction μ_s on common household floors was estimated to be ≥ 0.6 on dry linoleum, 0.5 on wet linoleum, and ≥ 0.55 on low-pile carpet, providing traction comparable

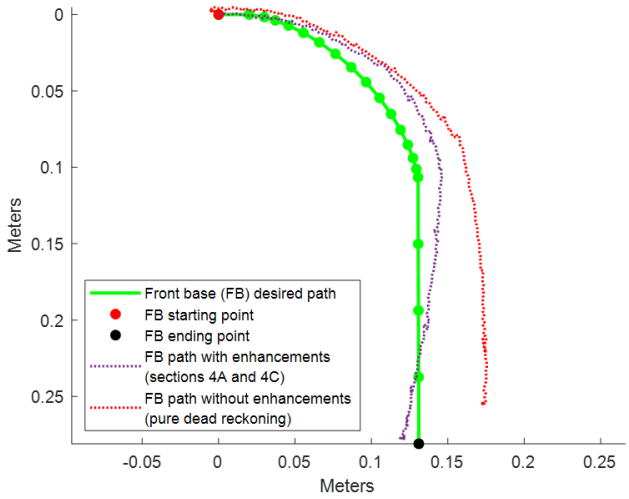

Fig. 8. Path tracking performance of a 1:4 scale model of the robot, with a target velocity of 4 cm/s. This sample path (same as in Fig. 5) involves a right-hand turn that exerts significant shear force on the treads.

to a car tire [27]. Absolute encoders (Taiss 3590S) were added to joints B, C, and the base turntables O_1 and O_2, as shown in Fig. 7. This enabled real-time measurement of the relative pose of the frame and bases.

Consent is paramount in caregiving, so the robot was equipped with a directional microphone and speakers for bidirectional communication between the teleoperator and the user. To prevent collisions with the user's feet, each drive base was instrumented with a strip of LED lights that could change color depending on the base's motion, alerting the user to movement of the base. A trio of depth cameras (Intel D435) were used for navigation; one on the top of the frame served as a viewport for the teleoperator, and one on the front of each base leveraged depth measurements to stop the base before any collisions would occur. Finally, the robot was padded with elderly-safe plastic and foam covers, and any potential pinch points were covered.

A. Path Tracking Performance

Fig. 8 shows the performance of a functionally identical 1:4 scale model of the robot in tracking the 0.4 m long test path in Fig. 5, which was designed to exert shear force on the treads. An overhead camera system monitored a marker on the front base. The robot was tested both with (purple line) and without (red line) the path following and dead reckoning enhancements in section 4. Tracking fidelity was assessed using four metrics: deviation from end of path; maximum deviation from path; root mean square error (RMSE) of the measured vs. desired path; and percent time spent in corrective rotation. Lower values of the latter resulted in smoother motion, since at each correction (step 4 in section 4A), the drive base switched from translation to rotation.

The enhancements significantly improved the tracking fidelity, despite the shear force experienced during the turn. The deviation from the path terminus and the maximum path deviation decreased by 71% (from 0.05 m to 0.015 m) and 60% (from 0.045 m to 0.018 m), respectively. In accordance with the treads' tendency to slip when the base ICR radius is small, the majority of the error was introduced along the turn. The algorithm in section 4A reduced the amount of corrective rotation to 4.5% of the total trajectory time, performing up to 54% better than point and shoot. The RSME also fell by 67%, from 0.0308 m to 0.0102 m.

Fig. 9. Use cases: demonstration of the 2BB providing assistance with common activities of daily living. From left to right, the first row shows ambulation in a corridor, standing up in a bathtub, and stepping over a bathtub lip onto a slippery floor. Row 2 demonstrates standing up from a couch, using the robot as a walker, and sit-to-stand from a toilet. Row 3 demonstrates reaching up to grab an item from a shelf, and reaching down to grab an item from a drawer (shown from two different angles).

B. Use Case Studies

As a proof of concept, the robot was successfully teleoperated by an adult subject, with each drive base mapped to a 2D joystick. The operator learned to control the robot in a short amount of time (approx. 5 mins) and was able to navigate between doorways, desks, and other obstacles. Common household scenarios were enacted with an adult subject to assess the robot's physical and haptic support, shown in Fig. 9. These scenarios reflect the activities that elderly people have difficulty performing [14], especially getting out from a bathtub and reaching up or down for items, which were rated as the most challenging tasks around the home [14]. In each situation, the robot was able to provide postural assistance as intended, and decreased the subject's perceived effort for performing the task. In contrast, standard assistive devices such as walkers or canes can only provide assistance for ambulation (Fig. 9, top left and center) or standing, and are unsuitable for use in other activities of daily living [15]. Additionally, the robot frame successfully

TABLE II
SIT-TO-STAND TRANSITION DURATION USING A FRONTAL HANDLEBAR AT EACH USER'S PREFERRED HEIGHT

	Average Time (sec)	Standard deviation (sec)
Without handlebar	1.71	0.23
With handlebar	1.20	0.39

spanned household obstacles such as a coffee table, and extended the handlebar over the lip of a bathtub.

Eight persons older than 70 who reported issues with balance, movement, or muscle pain were shown the robot concept. Five were open to using the robot in their home [14], suggesting a receptive market for adoption. The other three expressed concerns about the long-term reliability of any robot system. The elderly persons were asked to perform a sit-to-stand transition with a frontal handlebar at their preferred height (Table 2), which was an equivalent scenario to sitting directly in front of the 2BB. There was a statistically significant decrease of 29.77% in the average time for the sit-to-stand transition. A one-tailed unequal variance (Welch) t test found the decrease to be significant relative to $\alpha = 0.05$, with a p-value of 0.0042. Additionally, the perceived difficulty decreased from 1.67 ± 0.58 (1 standard deviation) to 1.0 ± 0, on a scale of 1 to 5, with 1 being easiest. This preliminary data indicates that the handlebar was beneficial for the target group.

VI. CONCLUSION AND DISCUSSION

We have successfully developed an eldercare robot to assist with postural transitions around the home, with a novel form factor able to navigate obstacles and extend over objects. To our knowledge, this robot design is unique in eldercare and is both the slimmest eldercare robot and the only one able to bear the weight of a human far from the robot's base of support. We have additionally proposed a control scheme for robot navigation that integrates localization, path planning, and path tracking, yet is generalizable to all robots with a similar nonholonomic kinematic structure and significant wheel slippage.

We believe that the system could best be used to augment the work of caregivers in nursing homes and assisted living communities. When elderly residents call for help, the robot could handle simpler tasks like postural assistance, while more complex tasks, emergencies, and robot maintenance could managed by the caretakers. With this need in mind, future work involves fully exploiting the kinematic design of the robot to further improve path following, conducting trials with elderly persons, adjusting the robot dimensions to better fit the target environment, and improving the robot's ability to measure and respond to human intent.

ACKNOWLEDGMENTS

This material is supported by National Robotics Initiative grant #2133075 and the NSF Graduate Research Fellowship under grant #2141064. Human subject tests were reviewed and approved by the MIT Committee on the Use of Humans as Experimental Subjects under IRB number 2207000712.

REFERENCES

[1] Urban Inst., "The US population is aging," urban.org/policy-centers/cross-center-initiatives/program-retirement-policy/projects/data-warehouse/what-future-holds/us-population-aging (accessed Aug. 12, 2023).
[2] S. Marchese, "The Caregiver Shortage: Which States Are Doing Best," The Mesothelioma Center, asbestos.com/support/caregivers/shortage-by-state/ (accessed Aug. 12, 2023).
[3] A. Oldenburg, "Nationwide Caregiver Shortage Felt By Older Adults," AARP, aarp.org/caregiving/basics/info-2022/in-home-caregiver-shortage.html (accessed Aug. 12, 2023).
[4] J. Biden, "Executive Order on Increasing Access to High-Quality Care and Supporting Caregivers," The White House, Apr. 2023.
[5] G. Bardaro et al., "Robots for Elderly Care in the Home: A Landscape Analysis and Co-Design Toolkit," Int J of Soc Robotics, 2022.
[6] K. Barhydt and H. H. Asada, "A High-Strength, Highly-Flexible Robotic Strap for Harnessing, Lifting, and Transferring Humans," in IEEE Robotics and Automation Letters, vol. 8, no. 4, pp. 2110-2117, April 2023, doi: 10.1109/LRA.2023.3246389.
[7] P. Asgharian et al., "A Review on the Use of Mobile Service Robots in Elderly Care," Robotics, vol. 11, no. 6, p. 127, Nov. 2022.
[8] R. Agrigoroaie et al., "The ENRICHME Project: Lessons Learnt from a First Interaction with the Elderly", Social Robotics, 2016.
[9] V. Pasqui et al., "Proposed Generic Method to Assess Efficiency of Smart-Walkers", Impact Analysis of Solutions for Chronic Disease Prevention and Management, ICOST, 2012.
[10] R. Bolli, P. Bonato and H. Harry Asada, "A Handle Robot for Providing Bodily Support to Elderly Persons," 2023 IEEE/RSJ International Conference on Intelligent Robots and Systems (IROS), Detroit, MI, USA, 2023, pp. 122-129, doi: 10.1109/IROS55552.2023.10341348.
[11] I. Levine et al., "Grab Bar Use Influences Fall Hazard During Bathtub Exit," Human Factors, Dec. 2021.
[12] A. W. Divelbiss and J. T. Wen, "A path space approach to nonholonomic motion planning in the presence of obstacles," IEEE Transactions on Robotics and Automation, 1997.
[13] N. Gell et al., "Mobility device use in older adults and incidence of falls and worry about falling: findings from the 2011-2012 national health and aging trends study," J American Geriatrics Society, 2015.
[14] R. Bolli and H. Asada, "A Data-Driven Approach to Positioning Grab Bars in the Sagittal Plane for Elderly Persons," Late-Breaking Report, IEEE International Conference on Robot and Human Interactive Communication (RO-MAN), Busan, South Korea, 2023.
[15] L. Axtell and Y. Yasuda, "Assistive Devices and Home Modifications in Geriatric Rehabilitation," Clinics in Geriatric Medicine, 1993.
[16] H. Sveistrup et al., "Evaluation of Bath Grab Bar Placement for Older Adults," Technology and Disability, Jan. 2006.
[17] D. Johnson and J. Pauls, "Systemic stair step geometry defects, increased injuries, and public health plus regulatory responses," Contemporary Ergonomics and Human Factors, 2010.
[18] S. Chang et al., "Understanding stand-to-sit maneuver: implications for motor system neuroprostheses after paralysis," Journal of Rehabilitation Research and Development vol. 51,9, 2014.
[19] D. Biman et al., "Isometric pull-push strengths in workspace: 1. Strength profiles," Int. J of Occupational Safety and Ergonomics, 2004.
[20] A. W. Divelbiss et al., "Trajectory tracking control of a car-trailer system," IEEE Transactions on Control Systems Technology, 1997.
[21] M. Islam, X. Ding and Y. He, "A closed-loop dynamic simulation-based design method for articulated heavy vehicles with active trailer steering systems", Vehicle System Dynamics, 2012.
[22] Y. Kanayama et al., "A stable tracking control method for an autonomous mobile robot," Proceedings., IEEE International Conference on Robotics and Automation, Cincinnati, OH, USA, 1990.
[23] R. W. Brockett, "Asymptotic stability and feedback stabilization," Differential Geometric Control Theory 27.1, 1983
[24] R. Siegwart et al, "Introduction to Autonomous Mobile Robots, Second Edition," MIT Press, 2011.
[25] M. Theers and M. Singh, "Pure Pursuit", Github, thomasfermi.github.io/Algorithms-for-Automated-Driving/Control/PurePursuit.html (accessed Aug. 26, 2023).
[26] Y. Shi et al., "Path Tracking Control of Self-Reconfigurable Robot hTetro With Four Differential Drive Units," in IEEE Robotics and Automation Letters, vol. 5, no. 3, pp. 3998-4005, July 2020, doi: 10.1109/LRA.2020.2983683.
[27] H. Jin and M. Zhou, "On the road friction recognition based on the driving wheels deceleration," 2014 IEEE Conference and Expo Transportation Electrification Asia-Pacific, Beijing, China, 2014.